The Translation Invariant Contourlet-like Transform for Image Denoising

LIAN Qiu-Sheng[1] CHEN Shu-Zhen[1]

Abstract The contourlet transform with anisotropy and directionality is a new extension to the wavelet transform. Because of its filter bank structure, the contourlet transform is not translation-invariant. In this paper, we propose the translation-invariant contourlet-like transform (TICLT) with lower redundancy than both the nonsubsampled contourlet transform (NSCT) and the translation invariant contourlet transform (TICT). The TICLT is constructed by combining the translation invariant Laplacian pyramid and undecimated directional filter banks. The undecimated directional filter banks, which satisfy the perfect reconstruction condition, are designed by the mapping approach using one-dimensional fractional splines orthogonal filter banks as prototype filters. We evaluate the performance of the TICLT in image denoising. Some comparisons with the state-of-the-art denoising methods are given to illustrate the potential of the TICLT.

Key words Contourlet transform, translation invariant, Laplacian pyramid (LP), image denoising

The importance of wavelets in signal processing applications is widely acknowledged. Indeed, they provide optimal approximation for one-dimensional piecewise smooth functions, but they do not perform well in higher dimensions. This limitation has led to several new constructions that can handle the geometrical structures of images efficiently. These constructions build dictionaries of anisotropic basis functions with many more shapes and directions than the classical separable wavelets, and provide a sparse representation of edges in images. One of the most successful constructions is the curvelet proposed by Candes and Donoho[1−2], which achieves optimal approximation for 2-D piecewise smooth functions with discontinuities along C^2 edges. Inspired by the curvelets, Do and Vetterli developed the contourlet transform[3], which is constructed by combining the Laplacian pyramid (LP) and the directional filter bank (DFB). Due to downsampling in the two stages, the contourlet transform is shift-variant. However, translation invariance is a desirable feature in many imaging applications such as pattern recognition, edge detection, and image denoising[4−6]. In [4], the nonsubsampled contourlet transform (NSCT) was obtained by combining a nonsubsampled pyramid structure and the nonsubsampled DFBs (NSDFB). In [5], the translation invariant contourlet transform (TICT) was constructed by coupling the translation invariant pyramid with the translation invariant DFB. In the TICT scheme, there are four detail channels at each scale without downsampler. In [7], the nonsubsampled shearlet transform (NSST), which has similar frequency tiling with contourlet, was constructed by combining a nonsubsampled Laplacian pyramid decomposition and shearing filters. All of the three transforms (NSCT, TICT, and NSST) are translation invariant at the cost of high redundancy. The NSCT and the TICT have redundancy given by $1+\sum_{j=1}^{J}2^{l_j}$ and $1+4\times\sum_{j=1}^{J}2^{l_j}$, respectively, where l_j denotes the number of levels in the NSDFB at the j-th scale. The redundancy of NSST is the same as NSCT.

Inspired by the nonsubsampled contourlet transform[4] and the second generation curvelets[2], we propose the translation invariant contourlet-like transform (TICLT) in this paper, which is built upon low-redundancy translation invariant Laplacian pyramid (TILP) and NSDFB. The TICLT is a translation invariant and directional multiresolution expansion that has similar frequency partition as the second generation curvelet transforms. Based on the TICLT, we propose a new method for image denoising, and some comparisons with the best available denoising results reported in the published works will be given to illustrate the potential of the TICLT.

Received March 13, 2008; in revised form September 21, 2008
Supported by National Natural Science Foundation of China (60772079)
1. Institute of Information Science and Technology, Yanshan University, Qinhuangdao 066004, P. R. China
DOI: 10.3724/SP.J.1004.2009.00505

1 The translation invariant contourlet-like transform

The TICLT combines the low-redundancy TILP and NSDFBs as shown in Fig. 1 (a). The TILP provides multiresolution composition and NSDFB provides directional decomposition. First, the input image is separated into lowpass and highpass subbands by filters H_0 and G_0. The highpass subband is decomposed into several directional subbands by NSDFB. The lowpass subband is then split into a bandpass subband and a lower-pass subband by filters H and G. The bandpass subband is further decomposed into several directional subbands by NSDFB, while the lower-pass subband is downsampled by a factor 2 in the horizontal and vertical directions. This scheme can be iterated on the lower-pass subband. We refer to the pyramidal structure constructed by H_0, G_0, H, G, and the downsampler M as TILP. The structure of TICLT as shown in Fig. 1 (a) splits the 2-D frequency plane into the subbands illustrated in Fig. 1 (b). To ensure the translation invariant property, the lowpass filter H must obey Nyquist sampling criterion

$$H(\boldsymbol{\omega})=0 \text{ for } |\boldsymbol{\omega}|=\sqrt{\omega_1^2+\omega_2^2}>\frac{\pi}{2} \tag{1}$$

Using the basic principle in multi-dimensional multirate system[8], we can obtain the perfect reconstruction conditions of the TILP as

$$H_0^2(\boldsymbol{\omega})+G_0^2(\boldsymbol{\omega})=1 \tag{2}$$

and

$$G^2(\boldsymbol{\omega})+\frac{H^2(\boldsymbol{\omega})}{4}=1 \tag{3}$$

These filters are designed by using the raise cosine function in frequency domain. They can be written as

$$H(\boldsymbol{\omega})=\begin{cases}2\sqrt{\dfrac{1+\cos(4|\boldsymbol{\omega}|-\pi)}{2}}, & \dfrac{\pi}{4}<|\boldsymbol{\omega}|<\dfrac{\pi}{2}\\ 2, & |\boldsymbol{\omega}|\le\dfrac{\pi}{4}\\ 0, & |\boldsymbol{\omega}|\ge\dfrac{\pi}{2}\end{cases} \tag{4}$$

$$G(\boldsymbol{\omega}) = \begin{cases} \sqrt{\dfrac{1-\cos(4|\boldsymbol{\omega}|-\pi)}{2}}, & \dfrac{\pi}{4} < |\boldsymbol{\omega}| < \dfrac{\pi}{2} \\ 0, & |\boldsymbol{\omega}| \le \dfrac{\pi}{4} \\ 1, & |\boldsymbol{\omega}| \ge \dfrac{\pi}{2} \end{cases} \tag{5}$$

$H_0(\boldsymbol{\omega}) = H(\boldsymbol{\omega}/2)/2$ and $G_0(\boldsymbol{\omega}) = G(\boldsymbol{\omega}/2)$. It is easy to testify that the filters H, G, H_0, and G_0 satisfy (1) ∼ (3).

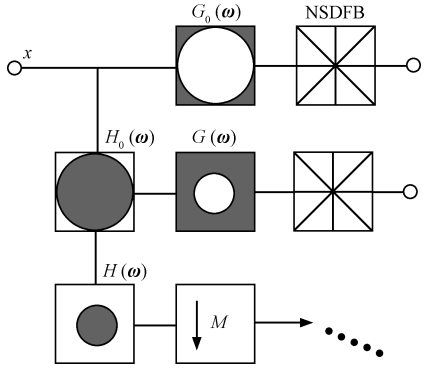

(a) The filter bank structure that implements the TICLT ($M = \mathrm{diag}\{2, 2\}$)

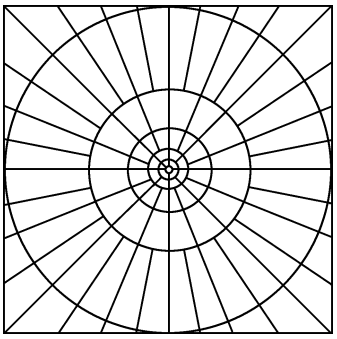

(b) The idealized frequency partitioning of TICLT

Fig. 1 The schematic diagrams of TICLT

The NSDFB in the TICLT is a nonsubsampled version of the critically sampled DFB[4, 9]. The building block of the NSDFB is a two-channel nonsubsampled fan filter bank (NSFFB) illustrated in Fig. 2. In this paper, the NSFFB is designed by the mapping approach using the 1-D fractional splines orthogonal filter bank

$$H_\lambda(\omega) = \frac{(2+2\cos\omega)^{\frac{\lambda}{2}}}{\sqrt{(2+2\cos\omega)^\lambda + (2-2\cos\omega)^\lambda}} \tag{6}$$

and

$$G_\lambda(\omega) = \frac{(2-2\cos\omega)^{\frac{\lambda}{2}}}{\sqrt{(2+2\cos\omega)^\lambda + (2-2\cos\omega)^\lambda}} \tag{7}$$

proposed in [10] as prototype filters, where λ is the continuously varying order parameter (in our implement, the best spacial-frequency resolution can be obtained when $\lambda = 10$). We can adjust the frequency responses of H_λ and G_λ by varying λ. As λ increases, these filters converge to the ideal half-band filters. Furthermore, H_λ is maximally flat at the origin. Applying the fan McClellan transform[11] to the 1-D fractional splines orthogonal filter bank, we obtain the complementary fan filters:

$$A(\boldsymbol{\omega}) = H_\lambda(\omega)|_{\cos\omega = M(\boldsymbol{\omega})} = \frac{(2+2M(\boldsymbol{\omega}))^{\frac{\lambda}{2}}}{\sqrt{(2+2M(\boldsymbol{\omega}))^\lambda + (2-2M(\boldsymbol{\omega}))^\lambda}} \tag{8}$$

$$B(\boldsymbol{\omega}) = G_\lambda(\omega)|_{\cos\omega = M(\boldsymbol{\omega})} = \frac{(2-2M(\boldsymbol{\omega}))^{\frac{\lambda}{2}}}{\sqrt{(2+2M(\boldsymbol{\omega}))^\lambda + (2-2M(\boldsymbol{\omega}))^\lambda}} \tag{9}$$

where $M(\boldsymbol{\omega})$ is the mapping function and $M(\boldsymbol{\omega}) = (\cos\omega_1 - \cos\omega_2)/2$. Fig. 3 shows the frequency response of the complementary fan filters for $\lambda = 10$. It is easy to show that the complementary fan filters satisfy the perfect reconstruction condition, that is,

$$A^2(\boldsymbol{\omega}) + B^2(\boldsymbol{\omega}) = 1 \tag{10}$$

Moreover, since the analysis and synthesis filters in the TICLT system are identical, they form a tight frame[12]. We can derive from (2), (3), and (10) that the frame bounds are equal to 1. In other words, the basis function $\varphi_{j,l,\boldsymbol{k}}$ of TICLT obeys Parseval relation $\sum_{j,l,k} |\langle f, \varphi_{j,l,\boldsymbol{k}}\rangle|^2 = \|f\|^2$, $\forall f \in L_2(\mathbf{Z}^2)$, where j is the scale parameter, l is the orientation parameter, and $\boldsymbol{k} = [k_1, k_2]$, $k_1, k_2 \in \mathbf{Z}$ is the translation parameter. Fig. 4 shows some basis functions of the TICLT. As the picture shows, these functions have a high degree of regularity, and offer good directional selectivity. The redundancy of the TICLT is $\sum_{j=1}^{2} 2^{l_j} + \sum_{j=3}^{J} 4^{-(j-2)} \times 2^{l_j} + 4^{-(J-1)}$, when $J > 2$, which is lower than those of the NSCT, NSST, and TICT.

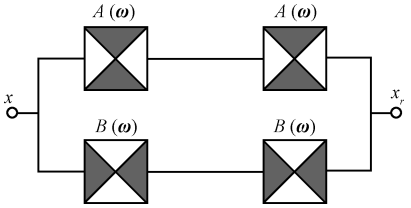

Fig. 2 The structure of the nonsubsampled fan filter bank

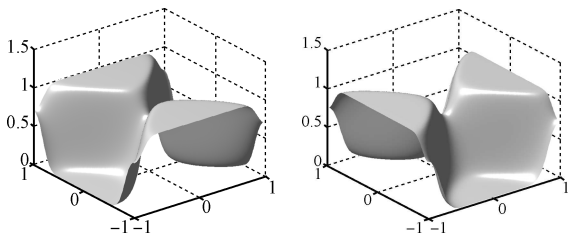

(a) The frequency response of $A(\boldsymbol{\omega})$ (b) The frequency response of $B(\boldsymbol{\omega})$

Fig. 3 The frequency response of the complementary fan filters

The main drawback of our construction is that the filters in the TICLT are not finite impulse response (FIR), so it may be costly to implement the transform. However, this drawback can be overcomed by using the fast Fourier transform (FFT) algorithm. In the following experiments, we implement the NSDFB in the Fourier domain, whereas the TILP in spacial domain with symmetric-padding extension mode.

The impulse responses of the filters in the TILP are obtained using the frequency-sampling approach. The four

filters in the TILP are zero-phase with 33×33 coefficients. We find that this implementation scheme improves the denoising performance of the TICLT slightly over the one that implements both the TILP and the NSDFB in Fourier domain.

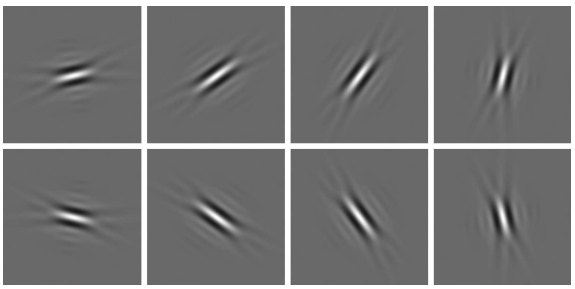

Fig. 4 Basis functions of the TICLT at scale 4

2 The image denoising algorithms based on the TICLT

In order to show the potential of the TICLT proposed in this paper, we applied it to remove additive white Gaussian noise (AWGN) by means of the hard-thresholding[13] and the minimum mean squared error (MMSE) estimator[14]. We refer to them as TICLT-HT and TICLT-MMSE, respectively. In our experiments, we used four scales of decomposition for the TICLT, and 8, 8, 16, 16 directions in the scales from coarser to finer, respectively. The continuously varying order parameter in (8) and (9) is fixed (i.e. $\lambda = 10$) to obtain the best spacial-frequency resolution.

For the hard-thresholding, we chose the global threshold $T_{j,l} = \beta\sigma_{nj,l}$ for each directional subband, where $\sigma_{nj,l}$ denotes the noise standard deviation of the directional subband at scale j and direction l. We set $\beta = 4$ for the finest scale and $\beta = 3$ for the others to get high peak signal to noise ratio (PSNR) and preserve more fine image details[4]. Since the TICLT is a nonorthogonal transform, the noise standard deviation $\sigma_{nj,l}$ should be estimated using Monte-Carlo simulations[3−4].

The TICLT-MMSE is illustrated as Fig. 5. For the MMSE estimator, each clean TICLT coefficient $x_{j,l,\boldsymbol{k}}$ was estimated by[14]

$$\hat{x}_{j,l,\boldsymbol{k}} = \frac{\sigma^2_{j,l,\boldsymbol{k}}}{\sigma^2_{j,l,\boldsymbol{k}} + \sigma^2_{nj,l}} y_{j,l,\boldsymbol{k}} \tag{11}$$

where $y_{j,l,\boldsymbol{k}}$ is the noisy observation of $x_{j,l,\boldsymbol{k}}$, and $\sigma^2_{j,l,\boldsymbol{k}}$ is the variance of the $\boldsymbol{k}$-th clean TICLT coefficients at the l-th directional subband of the j-th scale. It was assumed that $\sigma^2_{j,l,\boldsymbol{k}}$ is deterministic and known. But in fact, $\sigma^2_{j,l,\boldsymbol{k}}$ was unknown, so we used $\hat{\sigma}^2_{j,l,\boldsymbol{k}}$, which is an estimate of $\sigma^2_{j,l,\boldsymbol{k}}$. We set $\hat{\sigma}^2_{j,l,\boldsymbol{k}}$ equal to the variance of TICLT coefficients that were initially denoised by using the hard-thresholding estimator. That is, $\hat{\sigma}^2_{j,l,\boldsymbol{k}} = (1/S)\sum_{z_i \in N(\boldsymbol{k})} z_i^2$, where $N(\boldsymbol{k})$ is the neighborhood of $z_{j,l,\boldsymbol{k}}$, which is a "clean" TICLT coefficient of the denoised image using the hard-thresholding estimator, and S is the size of $N(\boldsymbol{k})$. In our experiments, we set S equals to 5×5.

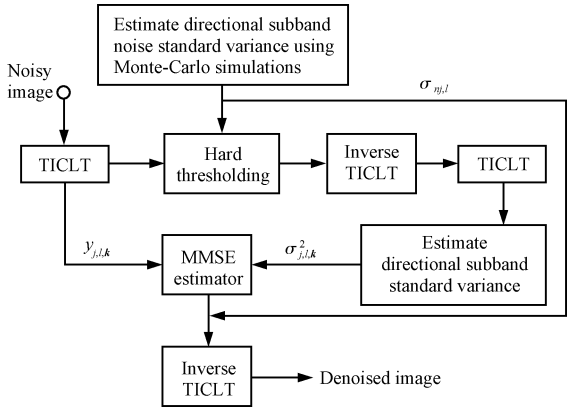

Fig. 5 The proposed TICLT-MMSE image denoising algorithm

3 Experiments

To benchmark the performance of the TICLT, we have used some of the best available denoising algorithms reported in the published works such as hard-thresholding in the undecimated wavelet transform domain (UWT-HT), hard-thresholding in the curvelet transform domain (CvT-HT)[15], hard-thresholding in the TICT domain (TICT-HT)[5], hard-thresholding in the NSCT domain (NSCT-HT)[4], local adaptive shrinkage in the NSCT domain (NSCT-LAS)[4], local adaptive shrinkage in the NSST1 $(16, 32)$ domain (NSST-LAS), and Bayes least-squares with a Gaussian scale-mixture model (BLS-GSM, this high complexity denoising algorithm is the benchmark used widely for evaluating different denoising methods)[16]. We used three 8-bit grayscale standard images of size 512×512 in our test suit: "Lena", "Barbara", and "Peppers". The results of these experiments are listed in Table 1 for three different levels of additive white Gaussian noise. The results showed that for the hard-thresholding estimator, the

Table 1 The PSNR values of the nine denoising methods (dB)

Image	Lena			Barbara			Peppers		
σ	10	20	30	10	20	30	10	20	30
Noisy	28.15	22.13	18.63	28.17	22.15	18.63	28.17	22.14	18.62
UWT-HT	34.26	31.40	29.66	31.58	27.23	25.10	33.71	31.19	29.43
CvT-HT	34.17	31.52	30.01	32.28	28.89	26.93	33.59	31.13	29.45
TICT-HT	34.89	31.75	—	33.49	29.53	—	34.00	31.15	—
NSCT-HT	34.69	32.03	30.35	33.01	29.41	27.24	33.81	31.60	30.07
TICLT-HT	**35.10**	**32.18**	**30.38**	**33.78**	**30.25**	**28.11**	**34.09**	**31.76**	**30.11**
NSCT-LAS	35.46	32.50	30.70	34.09	30.60	28.56	34.41	31.82	30.19
NSST-LAS	35.38	32.47	—	—	—	—	34.35	31.90	—
BLS-GSM	**35.59**	**32.62**	**30.84**	34.03	30.28	28.11	**34.63**	32.06	30.41
TICLT-MMSE	35.46	32.54	30.71	**34.24**	**30.73**	**28.59**	34.34	**32.07**	**30.45**

proposed TICLT outperforms other transforms in PSNR measure. The TICLT-MMSE obtains very encouraging results as well. In particular, the TICLT-MMSE yields the highest PSNR values for the "Barbara" image among the methods studied. The denoising results of the Barbara image are shown in Fig. 6. As the pictures show, the TICLT can preserve the edges and texture features of the original image effectively.

Since the complexity of MMSE is comparative with local adaptive shrinkage, moreover, the redundancy of the TICLT is lower than those of NSCT and NSST, and the computation complexity of TICLT-MMSE is also lower than those of NSCT-LAS and NSST-LAS.

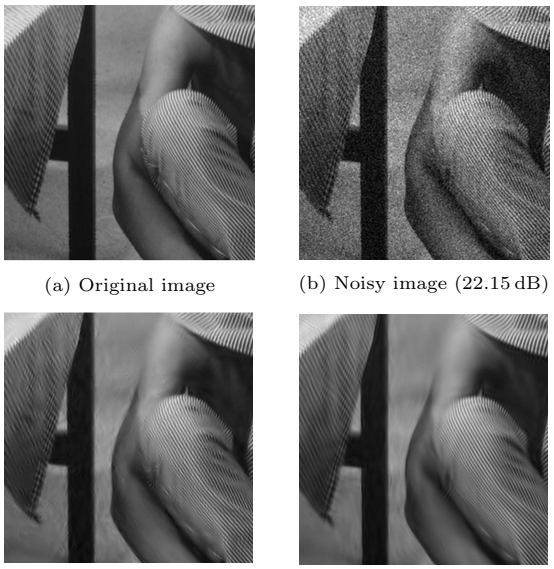

(a) Original image (b) Noisy image (22.15 dB)

(c) The result of BLS-GSM (30.28 dB) The result of TICLT-MMSE (30.73 dB)

Fig. 6 Denoising results for the Barbara images (cropped to 256×256) at $\sigma = 20$

4 Conclusion and future research

In this paper, we have proposed the translation invariant contourlet-like transform with lower redundancy than both the NSCT and the TICT. The potential of the TICLT has been demonstrated with some denoising examples. For the hard-thresholding, our results show that the TICLT outperforms other transforms such as UWT, CvT, TICT, and NSCT. For the TICLT-MMSE, better performance can be achieved at some cases when compared to the state-of-the-art denoising methods. Besides image denoising using TICLT, other inverse image problems (such as image debluring, super-resolution, compressed sensing[17], etc), which use the priors of sparseness when the image is represented by translation invariant transforms, will benefit with the use of TICLT. We intend to study some of these applications in future research.

References

1 Candes E J, Donoho D L. Curvelets: a surprisingly effective nonadaptive representation for objects with edges. In: Proceedings of the 4th International Conference on Curve and Surface. Saint-Malo, France: Vanderbilt University Press, 1999. 105−120

2 Candes E J, Guo F. New multiscale transforms, minimum total variation synthesis: application to edge-preserving image reconstruction. *Signal Processing*, 2002, **82**(11): 1519−1543

3 Do M N, Vetterli M. The contourlet transform: an efficient directional multiresolution image representation. *IEEE Transactions on Image Processing*, 2005, **14**(12): 2091−2106

4 da Cunha A L, Zhou J P, Do M N. The nonsubsampled contourlet transform: theory, design and applications. *IEEE Transactions on Image Processing*, 2006, **15**(10): 3089−3101

5 Eslami R, Radha H. Translation-invariant contourlet transform and its application to image denoising. *IEEE Transactions on Image Processing*, 2006, **15**(11): 3362−3374

6 Simoncelli E P, Freeman W T, Adelson E H, Heeger D J. Shiftable multiscale transforms. *IEEE Transactions on Information Theory*, 1992, **38**(2): 587−607

7 Easley G, Labate D, Lim W Q. Sparse directional image representations using the discrete shearlet transform. *Applied and Computational Harmonic Analysis*, 2008, **25**(1): 25−46

8 Vaidyanathan P P. *Multirate Systems and Filter Banks*. New York: Prentice Hall, 1993

9 Bamberger R H, Smith M J T. A filter bank for the directional decomposition of images: theory and design. *IEEE Transactions on Signal Processing*, 1992, **40**(4): 882−893

10 Feilner M, Van De Ville D, Unser M. An orthogonal family of quincunx wavelets with continuously adjustable order. *IEEE Transactions on Image Processing*, 2005, **14**(4): 499−510

11 McClellan J H. The design of two-dimensional digital filters by transformation. In: Proceedings of the 7th Annual Princeton Conference on Information Sciences and Systems. New Jersey, USA: IEEE, 1973. 247−251

12 Cvetkovic Z, Vetterli M. Oversampled filter banks. *IEEE Transactions on Signal Processing*, 1998, **46**(5): 1245−1255

13 Donoho D L, Johnstone I M. Ideal spatial adaptation by wavelet shrinkage. *Biometrika*, 1994, **81**(3): 425−455

14 Mihcak M K, Kozintsev I, Ramchandran K, Moulin P. Low complexity image denoising based on statistical modeling of wavelet coefficients. *IEEE Signal Processing Letters*, 1999, **6**(12): 300−303

15 Starck J L, Candes E J, Donoho D L. The curvelet transform for image denoising. *IEEE Transactions on Image Processing*, 2002, **11**(6): 670−684

16 Portilla J, Strela V, Wainwright M J, Simoncelli E P. Image denoising using scale mixtures of Gaussians in the wavelet domain. *IEEE Transactions on Image Processing*, 2003, **12**(11): 1338−1351

17 Donoho D L. Compressed sensing. *IEEE Transactions on Information Theory*, 2006, **52**(4): 1289−1306

LIAN Qiu-Sheng Associate professor at the Institute of Information Science and Technology, Yanshan University. He received his Ph. D. degree from Yanshan University in 2006. His research interest covers image processing, compressed sensing, and multiscale geometrical analysis. Corresponding author of this paper.
E-mail: lianqs@ysu.edu.cn

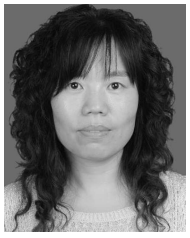

CHEN Shu-Zhen Lecturer at the Institute of Information Science and Technology, Yanshan University. Her research interest covers image processing, compressed sensing, and biometrics recognition.
E-mail: chen_sz818@163.com